

# Floquet engineering of topological localization transitions in non-Hermitian quasicrystals

Longwen Zhou<sup>1,\*</sup>

<sup>1</sup>College of Physics and Optoelectronic Engineering,  
Ocean University of China, Qingdao, China 266100

(Dated: 2021-11-09)

Time-periodic driving fields could endow a system with peculiar topological and transport features. In this work, we find dynamically controlled localization transitions in non-Hermitian quasicrystals via shaking the lattice periodically. The driving force is found to dress the hopping amplitudes between lattice sites, yielding alternate transitions between localized and extended non-Hermitian quasicrystalline phases. We apply our Floquet engineering approach to three representative Aubry-André-Harper non-Hermitian quasicrystals, and obtain the conditions of “photon-assisted” localization transitions and the expressions of Lyapunov exponents analytically. We further introduce topological winding numbers of Floquet quasienergies to distinguish non-Hermitian quasicrystalline phases with different localization nature. Our discovery thus extend the study of quasicrystals to non-Hermitian Floquet systems, and provide an effective way of modulating the topological and transport properties of these unique phases.

## I. INTRODUCTION

Floquet engineering has enabled the realization of rich dynamical, topological and transport phenomena in a broad range of physical settings [1–17]. Some notable examples include the dynamical localization, Floquet topological phase and discrete time crystal (see [18–30] for reviews and references therein). These discoveries have broadened the classification of phases of matter in nonequilibrium situations [31–33], and may find applications in emerging technologies like ultrafast electronics [22] and topological quantum computing [34–36].

Recently, the Floquet approach has been applied to engineer topological phases in non-Hermitian systems. Notably, it was found that the interplay between time-periodic driving fields and gain and loss or nonreciprocal effects could yield topological phases that are unique to non-Hermitian Floquet systems [37–44]. These intriguing phases of matter are characterized by large integer or half-integer winding numbers and degenerate Floquet edge or corner states with real quasienergies [37–43]. Their topological signatures may further be extracted experimentally from the dynamical spin textures and quantized displacements of wavepackets [44]. Till now, various kinds of non-Hermitian Floquet topological insulators, superconductors and semimetals with exceptional topological properties have been found [37–65]. Meanwhile, much less is known when non-Hermitian Floquet systems are subject to more complicated correlation effects, such as disorder, nonlinearity and many-body interactions.

In this work, we employ the idea of Floquet engineering to induce and control the spectrum, localization and topological transitions in non-Hermitian quasicrystals. A quasicrystal is a phase of matter with long-range order in the absence of spatial periodicity. It can be realized in a

lattice with diagonal or off-diagonal spatially quasiperiodic modulations. In Sec. II, we outline the method of adjusting hopping amplitudes in a tight-binding lattice by high-frequency periodic driving force, which follows the idea of engineering dynamical localization in ultracold atoms [1–3]. In Sec. III, we introduce three prototypical models of non-Hermitian quasicrystal, which can all be viewed as non-Hermitian variants of the Aubry-André-Harper (AAH) model. We further apply high-frequency shaking forces to these models, and obtain driving-induced transitions between non-Hermitian Floquet quasicrystalline phases with distinct transport and topological features. Different types of non-Hermitian quasicrystal phases are also found to emerge alternately with the increase of the ratio between the amplitude and frequency of the driving field. In Sec. IV, we summarize our results and discuss further perspectives.

## II. METHOD

In this section, we introduce our scheme of Floquet engineering to control the phase transitions in non-Hermitian quasicrystals, which is based on the idea of realizing dynamical localization in Bose-Einstein condensates [19]. A schematic illustration of our system and approach is shown in Fig. 1. The Hamiltonian of the system describes a tight-binding superlattice with onsite quasiperiodic potential and driving field, i.e.,

$$\hat{H}(t) = \sum_{\langle n, n' \rangle} \left( J_R \hat{c}_n^\dagger \hat{c}_{n'} + J_L \hat{c}_{n'}^\dagger \hat{c}_n \right) + \sum_n [V_n + W_n(t)] \hat{c}_n^\dagger \hat{c}_n, \quad (1)$$

where  $n$  is the lattice site index, and  $\langle n, n' \rangle$  refers to nearest-neighbor sites with  $n' > n$ .  $\hat{c}_n^\dagger$  and  $\hat{c}_n$  denote the creation and annihilation operators of a particle (either

\* zhoulw13@u.nus.edu

boson or fermion) on the  $n$ th lattice site.  $J_L$  ( $J_R$ ) represents the hopping amplitude of the particle from lattice site  $n$  ( $n'$ ) to  $n'$  ( $n$ ). A quasicrystal model is realized by setting the superlattice potential  $V_n$  to a quasiperiodic function of the lattice index  $n$ . A non-Hermitian quasicrystal is further obtained by setting  $J_L \neq J_R^*$  (for nonreciprocal hopping) or  $V_n \neq V_n^*$  (for gain and loss of particles). The coupling between the driving field and the particle takes the form of  $W_n(t) = -nF(t)$ , where the driving force  $F(t) = F(t + T)$  varies periodically in time with the driving period  $T$  and driving frequency  $\omega = 2\pi/T$ . All system parameters have been properly rescaled and given in dimensionless units. We will also set the Planck constant  $\hbar = 1$  throughout the discussion.

In the frame comoving with the lattice, the dynamics of the system is governed by the time-dependent Schrödinger equation

$$i\frac{d}{dt}|\psi(t)\rangle = \hat{H}(t)|\psi(t)\rangle. \quad (2)$$

The driving potential in  $\hat{H}(t)$  can be transformed to an oscillating phase factor in the hopping amplitudes  $J_{L,R}$  [19]. To do so, we introduce the following unitary rotation

$$\hat{R}(t) = e^{i\sum_n f_n(t)\hat{c}_n^\dagger \hat{c}_n}, \quad (3)$$

where the time-dependent amplitude

$$\begin{aligned} f_n(t) &= -\int_{t_0}^t W_n(t')dt' - n\bar{f} \\ &= n \left( \int_{t_0}^t F(t')dt' - \bar{f} \right) \equiv n f(t). \end{aligned} \quad (4)$$

Here  $\bar{f}$  is chosen to ensure that the one-period average of amplitude  $\frac{1}{T} \int_0^T f_n(t)dt = 0$ . Writing the time-evolving state as  $|\psi(t)\rangle = \hat{R}(t)|\psi'(t)\rangle$ , we obtain the Schrödinger

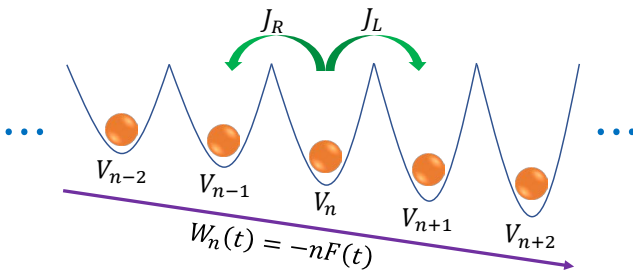


FIG. 1. A schematic illustration of the driven non-Hermitian superlattice.  $J_L$  ( $J_R$ ) denotes the hopping amplitude from left (right) to right (left) lattice sites.  $V_n$  denotes the static potential on the  $n$ th lattice site, which introduces quasiperiodicity into the system.  $W_n(t)$  is the driving potential, which is proportional to the position index  $n$ . The driving force  $F(t)$  oscillates periodically in time. The system is made non-Hermitian if  $J_L \neq J_R^*$  or  $V_n \neq V_n^*$ , corresponding to the case with nonreciprocal hopping or onsite gain and loss.

equation for the state  $|\psi'(t)\rangle$  in the rotating frame as

$$i\frac{d}{dt}|\psi'(t)\rangle = \hat{H}_r(t)|\psi'(t)\rangle, \quad (5)$$

where the Hamiltonian in the rotating frame  $\hat{H}_r(t)$  reads

$$\hat{H}_r(t) = \hat{R}^\dagger(t)\hat{H}(t)\hat{R}(t) - i\hat{R}^\dagger(t)\frac{d\hat{R}(t)}{dt}. \quad (6)$$

Plugging Eqs. (3) and (4) into Eq. (6), we find that  $\hat{R}(t)$  commutes with the onsite terms  $\sum_n [V_n + W_n(t)]\hat{c}_n^\dagger \hat{c}_n$  in  $\hat{H}(t)$  and

$$i\hat{R}^\dagger(t)\frac{d\hat{R}(t)}{dt} = \sum_n W_n(t)\hat{c}_n^\dagger \hat{c}_n, \quad (7)$$

which cancels the driving potential  $\sum_n W_n(t)\hat{c}_n^\dagger \hat{c}_n$ , leaving  $\sum_n V_n \hat{c}_n^\dagger \hat{c}_n$  as the only onsite term in  $\hat{H}_r(t)$ . Furthermore, the hopping terms in  $\hat{H}(t)$  under the rotation  $\hat{R}(t)$  becomes

$$\begin{aligned} \hat{R}^\dagger(t)\hat{c}_n^\dagger \hat{c}_{n'}\hat{R}(t) &= e^{-inf(t)\hat{c}_n^\dagger \hat{c}_n}\hat{c}_n^\dagger e^{inf(t)\hat{c}_n^\dagger \hat{c}_n} \\ &\times e^{-in'f(t)\hat{c}_{n'}^\dagger \hat{c}_{n'}}\hat{c}_{n'}^\dagger e^{in'f(t)\hat{c}_{n'}^\dagger \hat{c}_{n'}} \\ &= e^{i(n'-n)f(t)}\hat{c}_n^\dagger \hat{c}_{n'}. \end{aligned} \quad (8)$$

Note that this result holds for both bosons and fermions. Therefore, the Hamiltonian in the rotating frame is

$$\begin{aligned} \hat{H}_r(t) &= \sum_{\langle n, n' \rangle} J_L e^{i(n-n')f(t)}\hat{c}_{n'}^\dagger \hat{c}_n \\ &+ \sum_{\langle n, n' \rangle} J_R e^{i(n'-n)f(t)}\hat{c}_n^\dagger \hat{c}_{n'} + \sum_n V_n \hat{c}_n^\dagger \hat{c}_n, \end{aligned} \quad (9)$$

where the oscillating phase factor  $f(t) = \int_{t_0}^t F(t')dt' - \bar{f}$ . When  $f(t)$  varies quickly in time, so that  $\hbar\omega \gg |J_{R,L}|$  and  $|V_n - V_{n'}|$  for  $|n - n'| = 1$ , its effect on  $\hat{H}_r(t)$  can be approximated by the average over a complete driving period  $T$  [19]. This corresponds to taking the zeroth order term in the high-frequency expansion of the Floquet Hamiltonian [66–68]. In this limit, the micromotion operator is approximated by the rotating frame transformation  $\hat{R}(t)$ , and the resulting Floquet effective Hamiltonian reads

$$\begin{aligned} \hat{H}_F &\approx \frac{1}{T} \int_0^T dt \hat{H}_r(t) \\ &= \sum_{\langle n, n' \rangle} \left( J_L^{\text{eff}} \hat{c}_{n'}^\dagger \hat{c}_n + J_R^{\text{eff}} \hat{c}_n^\dagger \hat{c}_{n'} \right) + \sum_n V_n \hat{c}_n^\dagger \hat{c}_n, \end{aligned} \quad (10)$$

where the “photon-dressed” hopping amplitudes  $J_L^{\text{eff}}$  and

$J_R^{\text{eff}}$  are given by

$$J_L^{\text{eff}} = \frac{1}{T} \int_0^T dt J_L e^{i(n-n')f(t)}, \quad (11)$$

$$J_R^{\text{eff}} = \frac{1}{T} \int_0^T dt J_R e^{i(n'-n)f(t)}. \quad (12)$$

The driving field thus introduces a control knob to the hopping amplitude, and thus the transport property of the non-Hermitian quasicrystal.

In experiments, one type of driving force that is relatively easy to engineer has the form of harmonic functions [1, 19], which can be introduced by shaking the lattice back and forth periodically [69–71] and described as  $F(t) = K \cos(\omega t)$ , where  $K$  is the driving amplitude and  $\omega$  is the driving frequency of the force. The factor  $f(t)$  in the Peierls phase for such a harmonic drive reads  $f(t) = K \sin(\omega t)/\omega$  according to Eq. (4). Working out the the integrals in Eqs. (11) and (12) with the help of the Bessel function expansion  $e^{ix \sin(y)} = \sum_{l=-\infty}^{\infty} \mathcal{J}_l(x) e^{ily}$ , we find  $J_{L,R}^{\text{eff}} = J_{L,R} \mathcal{J}_0((n'-n)K/\omega)$ , which is derived previously in the study of dynamical localization [69]. The Floquet effective Hamiltonian of the system under the high-frequency harmonic forcing now takes the form

$$\begin{aligned} \hat{H}_F &= \sum_{\langle n, n' \rangle} J_L \mathcal{J}_0 \left( (n' - n) \frac{K}{\omega} \right) \hat{c}_{n'}^\dagger \hat{c}_n \\ &+ \sum_{\langle n, n' \rangle} J_R \mathcal{J}_0 \left( (n' - n) \frac{K}{\omega} \right) \hat{c}_n^\dagger \hat{c}_{n'} + \sum_n V_n \hat{c}_n^\dagger \hat{c}_n. \end{aligned} \quad (13)$$

Since both the  $J_{L,R}$  and the Bessel function of first kind  $\mathcal{J}_0((n'-n)K/\omega)$  decays with the increase of hopping distance  $|n' - n|$ , we could reserve the hopping terms up to nearest-neighbor sites, yielding the following Floquet effective Hamiltonian

$$\hat{H}_F = \sum_n \mathcal{J}_0 \left( \frac{K}{\omega} \right) \left( J_R \hat{c}_n^\dagger \hat{c}_{n+1} + J_L \hat{c}_{n+1}^\dagger \hat{c}_n \right) + \sum_n V_n \hat{c}_n^\dagger \hat{c}_n. \quad (14)$$

In the Hermitian limit, we observe that the hopping amplitudes  $J_{L,R}$  are switched off at the zeros of  $\mathcal{J}_0(K/\omega)$ , which leads to the well-known phenomena of dynamical localization for any nonvanishing onsite potential  $V_n$  [1]. When the system becomes non-Hermitian and  $V_n$  is quasiperiodic, the competition between the energy scales of intersite tunneling and onsite trapping could result in localization-delocalization transitions caused by non-Hermitian effects. The presence of the driving field further generates an interplay between the field parameters ( $K, \omega$ ) and the non-Hermitian terms of the system, which is expected to yield richer phase diagrams and dynamically controlled transitions between different non-Hermitian quasicrystalline phases. These judgments will be demonstrated by explicit examples in the following section.

### III. RESULTS

In this section, we apply the Floquet engineering approach developed in Sec. II to three representative models of non-Hermitian quasicrystal, which can all be viewed as non-Hermitian variants of the Aubry-André-Harper (AAH) model [72–74]. The explicit forms of these models and the driving forces are introduced in Subsec. III A. Without the driving field, the conditions of localization transition for these models have been derived in previous studies. We reveal how these conditions are modified in the presence of high-frequency lattice shaking forces, and obtain analytical expressions for their corresponding Lyapunov exponents, which are now functions of both the driving amplitude and driving frequency. Our theoretical results are further verified by numerical calculations presented in Subsecs. III B–III D.

#### A. Non-Hermitian Floquet quasicrystal models

The AAH model is one of the standard models in the study of localization-delocalization transitions in one-dimensional (1D) quasiperiodic systems [72–74]. In the lattice representation, the Hamiltonian of the model takes the form

$$\hat{H}_0 = \sum_n [J (\hat{c}_n^\dagger \hat{c}_{n+1} + \text{h.c.}) + V \cos(2\pi\alpha n) \hat{c}_n^\dagger \hat{c}_n], \quad (15)$$

where  $J$  is the hopping amplitude and  $V$  is the amplitude of the onsite potential. By setting  $\alpha$  to be an irrational number, the superlattice potential  $V \cos(2\pi\alpha n)$  becomes quasiperiodic in the lattice index  $n$ , and the system described by  $\hat{H}_0$  forms a 1D quasicrystal. Thanks to the self-duality property of the AAH quasicrystal, it has been shown that the eigenstates of  $\hat{H}_0$  possess a delocalization-to-localization transition at  $V = 2J$  in the thermodynamic limit. When  $V < 2J$ , all eigenstates of  $\hat{H}_0$  are delocalized and the system is in an extended phase. When  $V > 2J$ , the correlated disorder due to the quasiperiodic potential becomes strong enough, such that all eigenstates of  $\hat{H}_0$  are localized and the system enters an insulator phase [74].

In recent years, the impact of non-Hermiticity on localization transitions in AAH-type quasicrystals has been explored [75–93]. The non-Hermitian effects are introduced by either setting the onsite quasiperiodic potential to be non-Hermitian [76, 77], or making the hopping amplitudes between adjacent lattice sites to be nonreciprocal [78, 79]. In all these models, it was found that the non-Hermitian terms could induce a  $\mathcal{PT}$ -transition of the energy spectrum from real to complex (or the opposite), together with a localization-delocalization transition of the eigenstates. These transitions could further be characterized by the quantized change of a winding number of the spectrum around certain base point of the complex energy plane [76–79].

Model index	Hopping amplitude	Onsite potential $V_n$	Driving force $W_n(t)$
M1	$J_L = J_R = J$	$Ve^{-i2\pi\alpha n}$	
M2		$V \cos(2\pi\alpha n + i\gamma)$	$-nK \cos(\omega t)$
M3	$J_L = Je^\gamma, J_R = Je^{-\gamma}$	$V \cos(2\pi\alpha n)$	

TABLE I. Definitions of the three periodically forced non-Hermitian quasicrystal models. In the second column,  $J_L$  and  $J_R$  are left-to-right and right-to-left hopping amplitudes between nearest-neighbor lattice sites.  $\gamma$  controls the asymmetry between the left and right hopping amplitudes in M3. In the third column,  $V$  is the amplitude of the onsite potential,  $i\gamma$  is an imaginary phase shift and  $\alpha$  is an irrational number. In the third column,  $n$  is the lattice site index,  $K$  is the driving amplitude and  $\omega$  is the driving frequency. All system parameters are set in dimensionless units.

In this work, to apply the Floquet engineering approach to induce and control phase transitions in three AAH non-Hermitian quasicrystal models. The time-dependent Hamiltonian of these models take the general form of Eq. (1), with the explicit expressions of hopping amplitude, onsite potential and driving force given in Table I. We will refer to these three models as M1, M2 and M3 for simplicity. In the high-frequency limit, the Floquet effective Hamiltonian of these models then take the formalism of Eq. (14), where the hopping amplitudes are controlled by the ratio of driving amplitude and driving frequency  $K/\omega$  through the Bessel function  $\mathcal{J}_0(K/\omega)$ . Since the localization-delocalization transition in the AAH model is originated from the competition between the energy scales of hopping  $J$  and onsite potential  $V$  [74], the “photon-dressed” hopping amplitude  $J_{L,R}\mathcal{J}_0(K/\omega)$  provides a flexible knob to tune the transitions between different non-Hermitian quasicrystalline phases of the system, as will be demonstrated in the following subsections.

### B. M1: Floquet spectrum, localization transition and topological invariant

Following Table I, the time-dependent Hamiltonian of the non-Hermitian quasicrystal M1 reads

$$\hat{H}_1(t) = \sum_n J (\hat{c}_n^\dagger \hat{c}_{n+1} + \text{h.c.}) + \sum_n [Ve^{-i2\pi\alpha n} - nK \cos(\omega t)] \hat{c}_n^\dagger \hat{c}_n, \quad (16)$$

which is non-Hermitian due to the complex onsite potential  $Ve^{-i2\pi\alpha n}$  and quasiperiodic when  $\alpha$  is irrational. Following the procedure of Sec. II, we find the Floquet effective Hamiltonian of the system under high-frequency driving as

$$\hat{H}_{1F} = \sum_n \left[ J\mathcal{J}_0\left(\frac{K}{\omega}\right) (\hat{c}_n^\dagger \hat{c}_{n+1} + \text{h.c.}) + Ve^{-i2\pi\alpha n} \hat{c}_n^\dagger \hat{c}_n \right]. \quad (17)$$

The hopping strength now depends on the ratio between the amplitude and frequency of the driving field, and can thus be controlled dynamically. Meanwhile, the effective

Hamiltonian  $\hat{H}_{1F}$  possesses the  $\mathcal{PT}$ -symmetry as  $V_n = V_{-n}^*$ , which means that its Floquet spectrum could be real in certain parameter regime.

The quasienergy eigenvalue equation of  $\hat{H}_{1F}$  is given by  $\hat{H}_{1F}|\psi\rangle = E|\psi\rangle$ . Inserting the single-particle state  $|\psi\rangle = \sum_n \psi_n \hat{c}_n^\dagger |0\rangle$  into the equation, we obtain the eigenvalue equation in the lattice representation as

$$J\mathcal{J}_0\left(\frac{K}{\omega}\right) (\psi_{n+1} + \psi_{n-1}) + Ve^{-i2\pi\alpha n} \psi_n = E\psi_n. \quad (18)$$

Here  $E \bmod 2\pi$  corresponds to the quasienergy of  $\hat{H}_{1F}$ . For a lattice of length  $L$  and under the periodic boundary condition (PBC), one can take a discrete Fourier transformation from lattice to momentum representations by expanding the amplitude  $\psi_n$  as

$$\psi_n = \frac{1}{\sqrt{L}} \sum_{m=1}^L \varphi_m e^{-i2\pi\alpha mn}. \quad (19)$$

The transformed eigenvalue equation in momentum space then reads

$$V\varphi_{n-1} + 2J\mathcal{J}_0\left(\frac{K}{\omega}\right) \cos(2\pi\alpha n) \varphi_n = E\varphi_n. \quad (20)$$

Following the method outlined in Ref. [77], it can be readily shown that when  $\alpha$  takes irrational values, the non-Hermitian Floquet quasicrystal M1 possesses a  $\mathcal{PT}$ -transition and a localization-delocalization transition under the condition

$$|V| = |J\mathcal{J}_0(K/\omega)|. \quad (21)$$

When  $|V| < |J\mathcal{J}_0(K/\omega)|$ , the hopping process dominates and all Floquet eigenstates of  $\hat{H}_{1F}$  are extended with vanishing Lyapunov exponents (diverging localization lengths). The quasienergy dispersion of  $\hat{H}_{1F}$  in this case takes the form of  $E(k) = 2J\mathcal{J}_0(K/\omega) \cos(k) \in \mathbb{R}$ , where  $k \in [0, 2\pi]$ . When  $|V| > |J\mathcal{J}_0(K/\omega)|$ , the quasiperiodic superlattice potential dominates, and all Floquet eigenstates of  $\hat{H}_{1F}$  are localized with the same Lyapunov exponent (inverse localization length)  $\lambda = -\ln |J\mathcal{J}_0(K/\omega)/V| > 0$ . The Floquet spectrum of the system in this case has the form of  $E(k) = 2J\mathcal{J}_0(K/\omega) \cos(k - i\lambda) \in \mathbb{C}$ , where  $k \in [0, 2\pi]$ . The

Phase	Extended	Localized
Condition	$ V  <  J\mathcal{J}_0(K/\omega) $	$ V  >  J\mathcal{J}_0(K/\omega) $
IPR	$\simeq 0$ for all states	$> 0$ for all states
Lyapunov exponent	$\lambda = \ln \left  \frac{V}{J\mathcal{J}_0(K/\omega)} \right $	$\begin{cases} < 0 & \text{Extended} \\ > 0 & \text{Localized} \end{cases}$
Quasienergy	$E(k) = 2J\mathcal{J}_0(K/\omega) \cos k$	$E(k) = 2J\mathcal{J}_0(K/\omega) \cos(k - i\lambda)$
Winding number	$w = \int_0^{2\pi} \frac{d\theta}{2\pi} \partial_\theta \ln \det[\hat{H}'_{1F}(\theta) - E_0]$	$\begin{cases} 0 & \text{Extended} \\ -1 & \text{Localized} \end{cases}$

TABLE II. Summary of the results for the non-Hermitian Floquet quasicrystal M1.  $J$  is the nearest-neighbor hopping amplitude,  $V$  is the amplitude of onsite non-Hermitian quasiperiodic potential,  $K$  is the driving amplitude,  $\omega$  is the driving frequency, and  $\mathcal{J}_0(K/\omega)$  denotes the Bessel function of first kind. The parameter  $k$  fills uniformly the range of  $[0, 2\pi]$ .  $\hat{H}'_{1F}(\theta)$  is obtained from  $\hat{H}_{1F}$  after taking the discrete Fourier transformation and introducing a phase twist  $e^{-i\theta}$  to its top-right corner matrix element in momentum representation.  $E_0$  is the base quasienergy.

extended and localized phases could be further distinguished by a topological winding number of the Floquet spectrum. With the momentum-space eigenvalue equation (20), we find the matrix elements of the system's Floquet effective Hamiltonian  $\hat{H}'_{1F}$  in momentum space to be

$$\begin{aligned} [\hat{H}'_{1F}]_{n,n} &= 2J\mathcal{J}_0\left(\frac{K}{\omega}\right) \cos(2\pi\alpha n) \quad n = 1, \dots, L; \\ [\hat{H}'_{1F}]_{n+1,n} &= [\hat{H}'_{1F}]_{1,L} = V, \quad n = 1, \dots, L-1. \end{aligned} \quad (22)$$

Multiplying the corner matrix element  $[\hat{H}'_{1F}]_{1,L}$  by a phase factor  $e^{-i\theta}$ , we obtain the effective Hamiltonian  $\hat{H}'_{1F}(\theta)$  under the twist boundary condition in momentum space. The spectral winding number of  $\hat{H}'_{1F}(\theta)$  can then be obtained following the construction of Ref. [79]. Such a winding number counts the number of times the Floquet spectrum of  $\hat{H}'_{1F}(\theta)$  winds around a base quasienergy  $E_0$  on the complex plane  $\text{Re}E - \text{Im}E$  when  $\theta$  changes from zero to  $2\pi$ . When the quasienergy spectrum is real (complex), the value of this winding number is found to be zero ( $-1$ ). This winding number could thus serve as a topological order parameter to distinguish the extended phase (with real quasienergies) and localized phase (with complex quasienergies) of the system. In Table II, we summarize the key results about the spectrum, localization transition and topological invariant of the non-Hermitian Floquet quasicrystal M1. Notably, the condition of localization transition in the system now depends on the parameter  $K/\omega$  of the driving field. The states of the system can thus be tuned between extended and localized phases dynamically by varying the ratio  $K/\omega$  between the amplitude and frequency of the driving force.

To demonstrate our theoretical results, we compute the spectrum  $E$ , inverse participation ratio (IPR), Lyapunov exponent  $\lambda$  and winding number  $w$  of the M1 versus the amplitude of onsite potential  $V$  and the ratio between driving amplitude and frequency  $K/\omega$ . The numerical results are presented in Fig. 2. In the numerical calcula-

tion, we choose the undressed hopping amplitude  $J = 1$  and the quasicrystal parameter  $\alpha = \frac{\sqrt{5}-1}{2} \simeq \frac{p}{q}$ , with  $p, q$  being two adjacent elements of the Fibonacci sequence ( $p < q$ ). The length of lattice is chosen as  $L = 610$ , and the base quasienergy is set as  $E_0 = 0$ . In Fig. 2(a), we show the maximal imaginary parts of quasienergy  $\max|\text{Im}E|$  versus  $V$  and  $K/\omega$ . The red dashed line is given by the phase boundary equation  $|V| = |J\mathcal{J}_0(K/\omega)|$ . It is clear that  $\max|\text{Im}E| = 0$  ( $\max|\text{Im}E| > 0$ ) when  $|V| < |J\mathcal{J}_0(K/\omega)|$  ( $|V| > |J\mathcal{J}_0(K/\omega)|$ ). The condition  $|V| = |J\mathcal{J}_0(K/\omega)|$  thus determines the boundary of

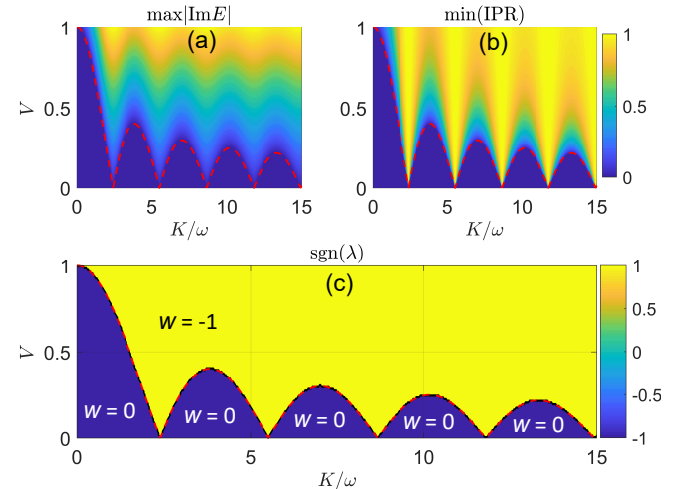


FIG. 2. The maximal imaginary parts of Floquet quasienergies in panel (a), the minimal values of IPRs in panel (b), and the signs of Lyapunov exponents in panel (c) of the non-Hermitian Floquet quasicrystal M1. Other system parameters are set as  $\alpha = \frac{\sqrt{5}-1}{2}$ ,  $J = 1$ , and the length of lattice is taken as  $L = 610$ . The red dashed line in each figure panel denotes the boundary between the extended phase (with real quasienergies for all Floquet eigenstates) and the localized phase (with complex quasienergies for all Floquet eigenstates), which satisfies the condition  $|V| = |J\mathcal{J}_0(K/\omega)|$  (see Table II). The topological winding number  $w$  of each phase is denoted explicitly in panel (c).

the  $\mathcal{PT}$ -transition between real and complex quasienergy spectrum of the system.

For any normalized Floquet right eigenstate  $|\psi\rangle = \sum_n \psi_n \hat{c}_n^\dagger |0\rangle$  of  $\hat{H}_{1F}$ , with  $\sum_{n=1}^L |\psi_n|^2 = 1$ , we define its IPR as

$$\text{IPR} = \sum_{n=1}^L |\psi_n|^4. \quad (23)$$

The minimum of IPRs over all eigenstates at a fix set of system parameters then yields the  $\text{min}(\text{IPR})$ . In Fig. 2(b), we present the  $\text{min}(\text{IPR})$  versus  $V$  and  $K/\omega$ , which is found to be  $\simeq 0$  when  $|V| < |J\mathcal{J}_0(K/\omega)|$  (below the red dashed line) and  $> 0$  otherwise. Notably, the maximum of IPRs of all eigenstates is found to have the same dependence on  $V$  and  $K/\omega$ . Therefore, the system is indeed in the extended (localized) phase with all states being delocalized (localized) when  $|V| < |J\mathcal{J}_0(K/\omega)|$  ( $|V| > |J\mathcal{J}_0(K/\omega)|$ ). Finally, we present the signs of Lyapunov exponent  $\lambda = -\ln |J\mathcal{J}_0(K/\omega)/V|$  and the topological winding numbers  $w$  of M1 versus  $V$  and  $K/\omega$  in Fig. 2(c). It is clear that the winding number  $w = 0$  and  $w = -1$  in the extended phase with real quasienergies and localized phase with complex quasienergies, which are separated by the phase boundary  $|V| = |J\mathcal{J}_0(K/\omega)|$  (red dashed line). Therefore, it is verified that  $w$  could be utilized as a topological order parameter to discriminate the  $\mathcal{PT}$ -invariant extended phase and  $\mathcal{PT}$ -breaking localized phase of the non-Hermitian Floquet quasicrystal M1. Note that without the driving field, the phase boundary between the extended and localized states reduces to a point at  $V = J$ . The driving force instead allows the localized phase to disappear and reappear alternately with the change of the driving parameter  $K/\omega$ , which highlights the advantage of Floquet engineering in the realization and control of phase transitions in non-Hermitian quasicrystals.

### C. M2: Floquet spectrum, localization transition and topological invariant

We next consider a driven non-Hermitian AAH quasicrystal with an imaginary phase shift  $i\gamma$ , whose Hamiltonian takes the form of

$$\begin{aligned} \hat{H}_2(t) = & \sum_n J (\hat{c}_n^\dagger \hat{c}_{n+1} + \text{h.c.}) \\ & + \sum_n [V \cos(2\pi\alpha n + i\gamma) - nK \cos(\omega t)] \hat{c}_n^\dagger \hat{c}_n. \end{aligned} \quad (24)$$

According to the theory presented in Sec. II, the Floquet effective Hamiltonian of this non-Hermitian quasicrystal

M2 is given by

$$\begin{aligned} \hat{H}_{2F} = & \sum_n J \mathcal{J}_0 \left( \frac{K}{\omega} \right) (\hat{c}_n^\dagger \hat{c}_{n+1} + \text{h.c.}) \\ & + \sum_n V \cos(2\pi\alpha n + i\gamma) \hat{c}_n^\dagger \hat{c}_n. \end{aligned} \quad (25)$$

It is clear that the hopping amplitude is modified by the driving field and its magnitude could be controlled by the ratio between the amplitude and frequency of the driving force  $K/\omega$ . Besides, the  $\hat{H}_{2F}$  also holds the  $\mathcal{PT}$ -symmetry, since its onsite potential  $V_n = V \cos(2\pi\alpha n + i\gamma) = V_{-n}^*$ . The Floquet quasienergy spectrum of  $\hat{H}_{2F}$  could then take real values in certain parameter regions.

Plugging the single-particle state  $|\psi\rangle = \sum_n \psi_n \hat{c}_n^\dagger |0\rangle$  into the eigenvalue equation  $\hat{H}_{2F}|\psi\rangle = E|\psi\rangle$  of the effective Hamiltonian, we obtain

$$J \mathcal{J}_0 \left( \frac{K}{\omega} \right) (\psi_{n+1} + \psi_{n-1}) + V \cos(2\pi\alpha n + i\gamma) \psi_n = E \psi_n, \quad (26)$$

where  $E \bmod 2\pi$  refers to the quasienergy. Taking the PBC for a finite lattice of length  $L$  and performing the discrete Fourier transformation by Eq. (19), we find the eigenvalue equation in momentum space to be

$$\frac{V}{2} (e^{i\gamma} \varphi_{n-1} + e^{-i\gamma} \varphi_{n+1}) + 2J \mathcal{J}_0 \left( \frac{K}{\omega} \right) \cos(2\pi\alpha n) \varphi_n = E \varphi_n, \quad (27)$$

which can also be viewed formally as a quasiperiodic lattice with nonreciprocal hopping and “photon-dressed” onsite potential.

Following the method developed in Ref. [76], it is straightforward to show that the non-Hermitian Floquet quasicrystal M2 could undergo a  $\mathcal{PT}$ -transition and a localization-delocalization transition when its parameters satisfy the condition

$$|V| e^{|i\gamma|} = |2J \mathcal{J}_0(K/\omega)|, \quad (28)$$

which is clearly dependent on the parameters of the driving field  $K$  and  $\omega$ . If  $|V| e^{|i\gamma|} < |2J \mathcal{J}_0(K/\omega)|$ , the hopping energy overwhelms the quasiperiodic onsite disorder, and the system sits in an extended phase. All Floquet eigenstates of the system in this phase have real quasienergies and delocalized profiles (with vanishing IPRs) throughout the lattice. If  $|V| e^{|i\gamma|} > |2J \mathcal{J}_0(K/\omega)|$ , the non-Hermitian onsite potential governs the behavior of the system and drives it into a localized phase. The Floquet states of the system in this phase are all localized (with finite IPRs) and have complex quasienergies. These localized eigenstates are found to share the common Lyapunov exponent  $\lambda = -\ln |2J \mathcal{J}_0(K/\omega)/(V e^{|i\gamma|})|$ , whose value is also controlled by the ratio between the amplitude and frequency of the driving force. To construct a topological winding number for M2, we introduce a real phase shift to the quasiperiodic onsite potential [76] by setting  $\cos(2\pi\alpha n + i\gamma) \rightarrow \cos(2\pi\alpha n + i\gamma + \theta/L)$  in Eq. (25),

Phase	Extended	Localized
Condition	$ V e^{ \gamma } <  2J\mathcal{J}_0(K/\omega) $	$ V e^{ \gamma } >  2J\mathcal{J}_0(K/\omega) $
IPR	$\simeq 0$ for all states	$> 0$ for all states
Lyapunov exponent	$\lambda = \ln \left  \frac{V e^{ \gamma }}{2J\mathcal{J}_0(K/\omega)} \right  \begin{cases} < 0 & \text{Extended} \\ > 0 & \text{Localized} \end{cases}$	
Quasienergy	Real	Complex
Winding number	$w = \int_0^{2\pi} \frac{d\theta}{2\pi} \partial_\theta \ln \det[\hat{H}_{2F}(\theta) - E_0] = \begin{cases} 0 & \text{Extended} \\ -1 & \text{Localized} \end{cases}$	

TABLE III. Summary of the results for the non-Hermitian Floquet quasicrystal M2.  $J$  is the nearest-neighbor hopping amplitude,  $V$  is the amplitude of onsite quasiperiodic potential,  $\gamma$  is the imaginary part of superlattice phase shift,  $K$  is the driving amplitude,  $\omega$  is the driving frequency, and  $\mathcal{J}_0(K/\omega)$  denotes the Bessel function of first kind.  $H_{2F}(\theta)$  is obtained from  $H_{2F}$  after setting  $V_n = V \cos(2\pi\alpha n + i\gamma + \theta/L)$ , with  $L$  being the length of lattice.  $E_0$  is the base quasienergy.

where  $L$  is the length of lattice. We denote the phase-shifted effective Hamiltonian by  $\hat{H}_{2F}(\theta)$ , and the number of times that its quasienergy spectrum winds around a base point  $E_0$  on the complex plane defines a topological invariant of the system, which is equal to  $-1$  when the spectrum is complex, and zero otherwise. Therefore, we conclude that the non-Hermitian Floquet quasicrystal M1 possesses an extended phase with real spectrum and winding number  $w = 0$ , and a localized phase with complex spectrum and winding number  $w = -1$ . By tuning the ratio  $K/\omega$  between the amplitude and frequency of the driving force, the system could also roam alternately between the  $\mathcal{PT}$ -invariant extended phase and the  $\mathcal{PT}$ -breaking topologically localized phase. The topological and transport properties of the non-Hermitian quasicrystal M2 could thus be controlled by the periodic driving field. We summarize the key results about the spectrum, phases and topological feature of M2 in Table III.

To verify our theoretical predictions, we compute the quasienergy spectrum, IPR, Lyapunov exponent and winding number of the non-Hermitian Floquet quasicrystal M2 numerically, with results reported in Fig. 3. In the calculation, we choose the system parameters  $(J, V) = (2, 1)$  and the quasiperiodic parameter  $\alpha = \frac{\sqrt{5}-1}{2} \simeq \frac{p}{q}$ , where  $p, q$  are two neighboring elements of the Fibonacci sequence ( $p < q$ ). The length of lattice is set as  $L = 610$ , and the base quasienergy is chosen to be  $E_0 = 0$ . In Fig. 3(a), we show the maximum of the imaginary parts of Floquet spectrum versus the parameter of driving force  $K/\omega$  and imaginary part of phase shift  $\gamma$ . The red-dashed line highlights the boundary of  $\mathcal{PT}$ -transition, which is determined by Eq. (28). The numerical results confirm that the Floquet spectrum of the system is indeed real when  $|V|e^{|\gamma|} < |2J\mathcal{J}_0(K/\omega)|$  (below the red-dashed line), and complex in other circumstances. In Fig. 3(b), we show the minimum of IPRs, which behaves similarly as the maximum of IPRs versus  $K/\omega$  and  $\gamma$  at each given set of system parameters. The results indicate that the IPRs of all states go to zero when  $|V|e^{|\gamma|} < |2J\mathcal{J}_0(K/\omega)|$  (below the red-dashed line), and become finite if  $|V|e^{|\gamma|} > |2J\mathcal{J}_0(K/\omega)|$ . Therefore, the condition in Eq. (28) defines the boundary between the

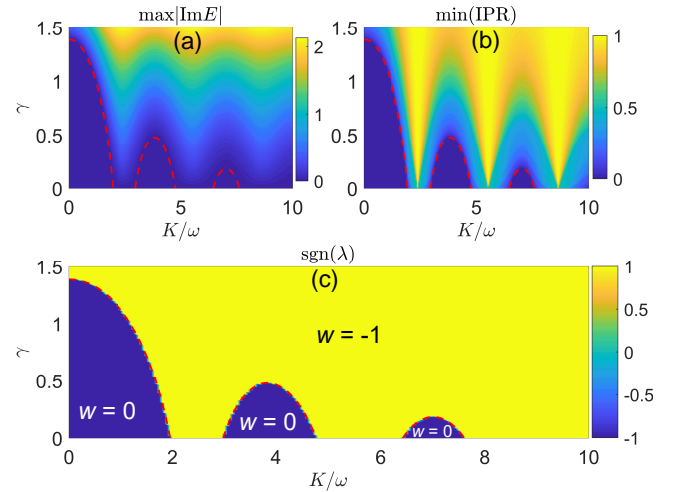


FIG. 3. The maximal imaginary parts of Floquet quasienergies in panel (a), the minimal values of IPRs in panel (b), and the signs of Lyapunov exponents in panel (c) of the non-Hermitian Floquet quasicrystal M2. Other system parameters are set as  $\alpha = \frac{\sqrt{5}-1}{2}$ ,  $J = 2$ ,  $V = 1$ , and the length of lattice is taken as  $L = 610$ . The red dashed line in each figure panel denotes the boundary between the extended phase (with real quasienergies for all Floquet eigenstates) and the localized phase (with complex quasienergies for all Floquet eigenstates), which satisfies the condition  $|V|e^{|\gamma|} = |2J\mathcal{J}_0(K/\omega)|$  (see Table II). The topological winding number  $w$  of each phase is denoted explicitly in panel (c).

$\mathcal{PT}$ -invariant extended phase and the  $\mathcal{PT}$ -breaking localized phase of the non-Hermitian Floquet quasicrystal M2. Finally, we show the signs of Lyapunov exponent  $\lambda$  and the topological winding numbers  $w$  versus  $K/\omega$  and  $\gamma$  in Fig. 3(c), in which we observe  $\lambda < 0$  ( $\lambda > 0$ ) for all states in the extended (localized) phase with  $w = 0$  ( $w = -1$ ), as shown by the blue (yellow) regions below (above) the phase boundary (i.e., the red-dashed line satisfying Eq. (28)). Therefore, the winding number  $w$  works as a topological invariant to distinguish the  $\mathcal{PT}$ -breaking localized phase and  $\mathcal{PT}$ -invariant extended phase of the system. Similar to the case of M1,

the driving force now allows one to change the system over a series of transitions between localized and delocalized phases. This further demonstrates the generality of our Floquet engineering approach to the design and control of non-Hermitian quasicrystalline phases in different model systems.

#### D. M3: Floquet spectrum, localization transition and topological invariant

In the last part of this section, we consider a non-reciprocal variant of the AAH model [78, 79], which is subject to a periodically modulated driving force. The time-dependent Hamiltonian of the model takes the form

$$\hat{H}_3(t) = \sum_n J \left( e^{-\gamma} \hat{c}_n^\dagger \hat{c}_{n+1} + e^{\gamma} \hat{c}_{n+1}^\dagger \hat{c}_n \right) + \sum_n [V \cos(2\pi\alpha n) - nK \cos(\omega t)] \hat{c}_n^\dagger \hat{c}_n, \quad (29)$$

which is non-Hermitian if  $\gamma \neq 0$ . Following the steps of Sec. II, we obtain the Floquet effective Hamiltonian of this non-Hermitian quasicrystal M3 under the high-frequency approximation as

$$\hat{H}_{3F} = \sum_n \mathcal{J}_0 \left( \frac{K}{\omega} \right) J \left( e^{-\gamma} \hat{c}_n^\dagger \hat{c}_{n+1} + e^{\gamma} \hat{c}_{n+1}^\dagger \hat{c}_n \right) + \sum_n V \cos(2\pi\alpha n) \hat{c}_n^\dagger \hat{c}_n. \quad (30)$$

The hopping amplitude is now controlled by the amplitude  $K$  and frequency  $\omega$  of the driving field. Applying  $\hat{H}_{3F}$  to the eigenstate  $|\psi\rangle = \sum_n \psi_n \hat{c}_n^\dagger |0\rangle$ , we further obtain the eigenvalue equation in lattice representation

$$\mathcal{J}_0 \left( \frac{K}{\omega} \right) J (e^{\gamma} \psi_{n-1} + e^{-\gamma} \psi_{n+1}) + V \cos(2\pi\alpha n) \psi_n = E \psi_n. \quad (31)$$

We observe that this equation takes the same form as Eq. (27), with the correspondence between system parameters  $V \leftrightarrow 2J\mathcal{J}_0(K/\omega)$ , which implies that the non-Hermitian Floquet quasicrystals M2 and M3 are dual with each other concerning their spectrum and eigenstates. Furthermore, taking the Fourier transformation of Eq. (31) with the help of Eq. (19), we obtain

$$\frac{V}{2} (\varphi_{n+1} + \varphi_{n-1}) + 2J\mathcal{J}_0 \left( \frac{K}{\omega} \right) \cos(2\pi\alpha n - i\gamma) \varphi_n = E \varphi_n, \quad (32)$$

which again shares the same form with Eq. (26) under the exchange of system parameters  $V \leftrightarrow 2J\mathcal{J}_0(K/\omega)$ . Putting together, we find that under the PBC, there is indeed a duality relation between the M2 and M3, in the sense that the localization properties of the M2 in momentum space is consistent with the localization properties of the M3 in position space under the PBC. With the help of this duality relation, we can immediately write

down the phase boundary condition that determines the  $\mathcal{PT}$ -transition and localization-delocalization transition in the non-Hermitian Floquet quasicrystal M3, i.e.,

$$|V| = |2J\mathcal{J}_0(K/\omega)|e^{|\gamma|}. \quad (33)$$

In parallel with the discussions of Subsec. III C, if  $|V| < |2J\mathcal{J}_0(K/\omega)|e^{|\gamma|}$ , the M3 is found to be in a  $\mathcal{PT}$ -breaking extended phase (dual to the localized phase of M2) with complex quasienergies and vanishing IPRs for all Floquet eigenstates. When  $|V| > |2J\mathcal{J}_0(K/\omega)|e^{|\gamma|}$ , the M3 is in a  $\mathcal{PT}$ -invariant localized phase (dual to the extended phase of M2), where all Floquet eigenstates have real quasienergies, finite IPRs, and the same positive Lyapunov exponent  $\lambda = -\ln |2J\mathcal{J}_0(K/\omega)e^{|\gamma|}/V|$  in the thermodynamic limit  $L \rightarrow \infty$ . Note that due to the dependence of phase boundary condition Eq. (33) and Lyapunov exponent on the ratio between the amplitude and frequency of the driving force  $K/\omega$ , transitions between phases with different spectrum and transport features in the M3 can also be induced by the driving field.

To define the spectral winding number, we take the twist boundary condition [79] by adding phase factors to the corner matrix elements of  $\hat{H}_{3F}$  in the lattice representation, i.e.,

$$[\hat{H}_{3F}]_{1,L} = J e^{(\gamma - i\theta)}, \quad [\hat{H}_{3F}]_{L,1} = J e^{(i\theta - \gamma)}, \quad (34)$$

where  $L$  is the length of lattice and  $\theta \in [0, 2\pi]$ . The spectrum of the phase-dependent Hamiltonian  $\hat{H}_{3F}(\theta)$  could now possess a winding number around certain base quasienergy  $E_0$  on the complex plane when  $\theta$  changes over a cycle from zero to  $2\pi$ . Such a winding number could be nonzero only if the quasienergy spectrum of  $\hat{H}_{3F}(\theta)$  is complex. Therefore, we expect a quantized winding number to appear for the  $\mathcal{PT}$ -breaking extended phase, and a vanishing one for the  $\mathcal{PT}$ -invariant localized phase of the system. Such a winding number can then be used as a topological invariant to distinguish the two non-Hermitian Floquet quasicrystalline phases of M3 with distinct spectrum and transport nature. We summarize our main results about the M3 in Table IV for the ease of reference.

To confirm our theoretical predictions, we present the Floquet spectrum, IPR, Lyapunov exponent and winding number of the M3 versus the imaginary part of phase shift  $\gamma$  and the ratio between the amplitude and frequency of driving field  $K/\omega$  in Fig. 4. Other system parameters are set as  $J = V = 1$  in the calculation. The quasicrystal parameter  $\alpha = \frac{\sqrt{5}-1}{2} \simeq \frac{p}{q}$ , with  $p, q$  being adjacent elements of the Fibonacci sequence ( $p < q$ ). The length of lattice is chosen to be  $L = 610$ , and the base quasienergy is set as  $E_0 = 0$ . In Figs. 4(a)–(c), the red dashed line refers to the phase boundary satisfying the Eq. (33). We observe that the maximum of imaginary parts of quasienergy  $\max(\text{Im}E)$  vanishes below the red dashed line and taking finite values above it, as shown in Figs. 4(a). The system thus undergoes a  $\mathcal{PT}$ -transition when  $|V|$  increase

Phase	Extended	Localized
Condition	$ V e^{- \gamma } <  2J\mathcal{J}_0(K/\omega) $	$ V e^{- \gamma } >  2J\mathcal{J}_0(K/\omega) $
IPR	$\simeq 0$ for all states	$> 0$ for all states
Lyapunov exponent	$\lambda = \ln \left  \frac{Ve^{- \gamma }}{2J\mathcal{J}_0(K/\omega)} \right $	$\begin{cases} < 0 & \text{Extended} \\ > 0 & \text{Localized} \end{cases}$
Quasienergy	Complex	Real
Winding number	$w = \int_0^{2\pi} \frac{d\theta}{2\pi} \partial_\theta \ln \det[H_{3F}(\theta) - E_0] = \begin{cases} -1 & \text{Extended} \\ 0 & \text{Localized} \end{cases}$	

TABLE IV. Summary of the results for non-Hermitian Floquet quasicrystal M3.  $J$  is the symmetric part of nearest-neighbor hopping amplitude,  $\gamma$  controls the asymmetry between left and right hopping amplitudes,  $V$  is the amplitude of onsite quasiperiodic potential,  $K$  is the driving amplitude,  $\omega$  is the driving frequency, and  $\mathcal{J}_0(K/\omega)$  denotes the Bessel function of first kind.  $H_{3F}(\theta)$  is obtained from  $H_{3F}$  after taking the periodic boundary condition and setting its top-right (bottom-left) corner matrix element to be  $J_L \mathcal{J}_0(K/\omega) e^{-i\theta}$  ( $J_R \mathcal{J}_0(K/\omega) e^{i\theta}$ ).  $E_0$  is the base quasienergy.

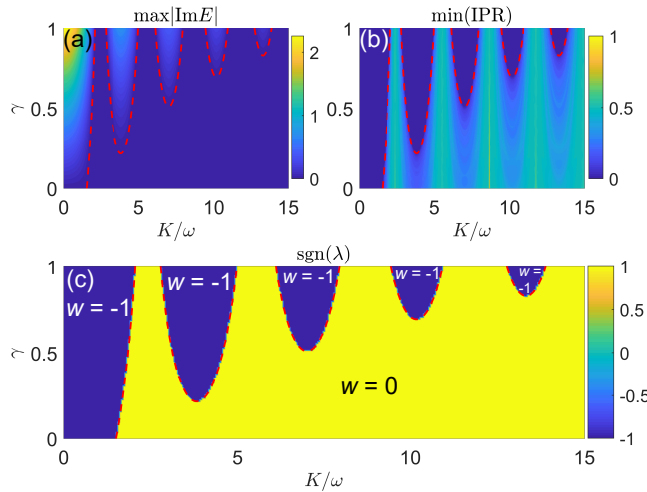


FIG. 4. The maximal imaginary parts of Floquet quasienergies in panel (a), the minimal values of IPRs in panel (b), and the signs of Lyapunov exponents in panel (c) of the non-Hermitian Floquet quasicrystal M3. Other system parameters are set as  $\alpha = \frac{\sqrt{5}-1}{2}$ ,  $J = 1$ ,  $V = 1$ , and the length of lattice is taken as  $L = 610$ . The red dashed line in each figure panel denotes the boundary between the extended phase (with complex quasienergies for all Floquet eigenstates) and the localized phase (with real quasienergies for all Floquet eigenstates), which satisfies the condition  $|V|e^{-|\gamma|} = |2J\mathcal{J}_0(K/\omega)|$  (see Table II). The topological winding number  $w$  of each phase is denoted explicitly in panel (c).

from below  $|2J\mathcal{J}_0(K/\omega)|e^{|\gamma|}$  to above it, through which the Floquet spectrum changes from complex to real. In Fig. 4(b), we show the minimum of IPRs  $\min(\text{IPR})$  over all Floquet eigenstates at each given set of system parameters. The maximum of IPRs versus  $K/\omega$  and  $\gamma$  are found to have the same pattern. Therefore, all states of the system are extended in the  $\mathcal{PT}$ -breaking regime (with complex spectrum), and localized in the  $\mathcal{PT}$ -invariant regime (with real spectrum). In Fig. 4(c), we show the signs of Lyapunov exponent  $\text{sgn}(\lambda)$  and winding numbers  $w$  of different phases. We obtain identical and pos-

itive (negative)  $\lambda$  for all states below (above) the phase boundary line, implying a phase with localized (delocalized) states at all quasienergies. Moreover, we find the winding number  $w = 0$  and  $w = -1$  in the localized and delocalized phases, respectively, and a quantized change of  $w$  across the phase boundary (red dashed line). The driven non-Hermitian quasicrystal M3 thus possesses a  $\mathcal{PT}$ -breaking extended phase with topological winding number  $w = -1$ , in which all Floquet eigenstates are delocalized with complex quasienergies, and a  $\mathcal{PT}$ -invariant localized phase with topological winding number  $w = 0$ , in which all Floquet eigenstates are localized with real quasienergies. As the phase boundary is controlled by the amplitude and frequency of the driving force, the system can also be tuned dynamically to go through transitions between different non-Hermitian quasicrystalline phases following our Floquet engineering scheme. Combining these observations with the results obtained in Subsecs. III B and III C, we conclude that our Floquet engineering strategy could be exploited as a useful means to control and modulate the spectrum, topological and transport properties for a broad class of non-Hermitian quasicrystals.

#### IV. SUMMARY

In this work, we apply Floquet driving fields to engineer  $\mathcal{PT}$ -breaking, localization-to-delocalization and topological transitions in non-Hermitian quasicrystals. Following the well-known scheme of dynamical localization, we utilize high-frequency shaking forces to control the hopping amplitudes of non-Hermitian quasiperiodic lattices, and observing alternate transitions between extended and localized phases with the change of driving field parameters. We implement our scheme in three prototypical models of non-Hermitian quasicrystal, and obtain the conditions of driving-induced  $\mathcal{PT}$ -transition and localization-delocalization transition in these systems. We further introduced winding numbers of the quasienergy spectrum to distinguish non-Hermitian Flo-

quet quasicrystals with different spectrum and localization features, and establishing the topological phase diagrams of these intriguing phases. Our results thus extend the study of non-Hermitian quasicrystals to periodically driven systems, and further uncover the usefulness of the Floquet engineering approach to the design and control of non-Hermitian quasicrystals with distinctive topological and transport properties.

In future work, it would be interesting to apply our scheme to the engineering of non-Hermitian quasicrystals with mobility edges [94], long-range hoppings, superconducting pairings, nonlinear effects, many-body interactions and in higher spatial dimensions. Under moderate driving frequencies, quasicrystalline phases that are unique to non-Hermitian Floquet systems may also emerge, which certainly deserve more thorough explo-

rations [94].

## ACKNOWLEDGMENTS

L.Z. is supported by the National Natural Science Foundation of China (Grant No. 11905211), the China Postdoctoral Science Foundation (Grant No. 2019M662444), the Fundamental Research Funds for the Central Universities (Grant No. 841912009), the Young Talents Project at Ocean University of China (Grant No. 861801013196), and the Applied Research Project of Postdoctoral Fellows in Qingdao (Grant No. 861905040009).

---

[1] H. Lignier, C. Sias, D. Ciampini, Y. Singh, A. Zenesini, O. Morsch, and E. Arimondo, Dynamical Control of Matter-Wave Tunneling in Periodic Potentials, *Phys. Rev. Lett.* **99**, 220403 (2007).

[2] F. L. Moore, J. C. Robinson, C. Bharucha, P. E. Williams, and M. G. Raizen, Observation of Dynamical Localization in Atomic Momentum Transfer: A New Testing Ground for Quantum Chaos, *Phys. Rev. Lett.* **73**, 2974 (1994).

[3] M. Bitter and V. Milner, Experimental Observation of Dynamical Localization in Laser-Kicked Molecular Rotors, *Phys. Rev. Lett.* **117**, 144104 (2016).

[4] M. C. Rechtsman, J. M. Zeuner, Y. Plotnik, Y. Lumer, D. Podolsky, F. Dreisow, S. Nolte, M. Segev, and A. Szameit, Photonic Floquet topological insulators, *Nature* **496**, 196-200 (2013).

[5] J. W. McIver, B. Schulte, F.-U. Stein, T. Matsuyama, G. Jotzu, G. Meier, and A. Cavalleri, Light-induced anomalous Hall effect in graphene, *Nat. Phys.* **16**, 38-41 (2020).

[6] S. Mukherjee and M. C. Rechtsman, Observation of Floquet solitons in a topological bandgap, *Science* **368**, 856-859 (2020).

[7] A. Darabi, X. Ni, M. Leamy, and A. Alù, Reconfigurable Floquet elastodynamic topological insulator based on synthetic angular momentum bias, *Sci. Adv.* **6**, eaba8656 (2020).

[8] W. Ma, L. Zhou, Q. Zhang, M. Li, C. Cheng, J. Geng, X. Rong, F. Shi, J. Gong, and J. Du, Experimental Observation of a Generalized Thouless Pump with a Single Spin, *Phys. Rev. Lett.* **120**, 120501 (2018).

[9] G. Jotzu, M. Messer, R. Desbuquois, M. Lebrat, T. Uehlinger, D. Greif, and T. Esslinger, Experimental realization of the topological Haldane model with ultracold fermions, *Nature* **515**, 237-240 (2014).

[10] K. Wintersperger, C. Braun, F. N. Ünal, A. Eckardt, M. Di Liberto, N. Goldman, I. Bloch, and M. Aidelsburger, Realization of an anomalous Floquet topological system with ultracold atoms, *Nat. Phys.* **16**, 1058-1063 (2020).

[11] A. Alberti, V. V. Ivanov, G. M. Tino, and G. Ferrari, Engineering the quantum transport of atomic wavefunctions over macroscopic distances, *Nat. Phys.* **5**, 547-550 (2009).

[12] C. Sias, H. Lignier, Y. P. Singh, A. Zenesini, D. Ciampini, O. Morsch, and E. Arimondo, Observation of Photon-Assisted Tunneling in Optical Lattices *Phys. Rev. Lett.* **100**, 040404 (2008).

[13] V. V. Ivanov, A. Alberti, M. Schioppo, G. Ferrari, M. Artoni, M. L. Chiofalo, and G. M. Tino, Coherent Delocalization of Atomic Wave Packets in Driven Lattice Potentials, *Phys. Rev. Lett.* **100**, 043602 (2008).

[14] E. Haller, R. Hart, M. J. Mark, J. G. Danzl, L. Reichsöllner, and H.-C. Nägerl, Inducing Transport in a Dissipation-Free Lattice with Super Bloch Oscillations, *Phys. Rev. Lett.* **104**, 200403 (2010).

[15] N. Poli, F.-Y. Wang, M. G. Tarallo, A. Alberti, M. Prevedelli, and G. M. Tino, Precision Measurement of Gravity with Cold Atoms in an Optical Lattice and Comparison with a Classical Gravimeter, *Phys. Rev. Lett.* **106**, 038501 (2011).

[16] R. Ma, M. E. Tai, P. M. Preiss, W. S. Bakr, J. Simon, and M. Greiner, Photon-Assisted Tunneling in a Biased Strongly Correlated Bose Gas, *Phys. Rev. Lett.* **107**, 095301 (2011).

[17] Y. Chen, S. Nascimbène, M. Aidelsburger, M. Atala, S. Trotzky, and I. Bloch, Controlling Correlated Tunneling and Superexchange Interactions with ac-Driven Optical Lattices, *Phys. Rev. Lett.* **107**, 210405 (2011).

[18] M. Grifoni and P. Hänggi, Driven quantum tunneling, *Phys. Rep.* **304** 229-354 (1998).

[19] A. Eckardt, *Colloquium: Atomic quantum gases in periodically driven optical lattices*, *Rev. Mod. Phys.* **89**, 011004 (2017).

[20] M. Holthaus, Floquet engineering with quasienergy bands of periodically driven optical lattices, *J. Phys. B: At. Mol. Opt. Phys.* **49**, 013001 (2016).

[21] G. Casati and L. Molinari, “Quantum Chaos” with Time-Periodic Hamiltonians, *Progress of Theoretical Physics Supplement* **98**, 287-322 (1989).

[22] T. Oka and S. Kitamura, Floquet Engineering of Quantum Materials, *Annu. Rev. Condens. Matter Phys.* **10**, 387-408 (2019).

[23] J. Cayssol, B. Dóra, F. Simon, and R. Moessner, Floquet topological insulators, *Phys. Status Solidi RRL*, **7**, 101-108 (2013).

[24] F. Harper, R. Roy, M. S. Rudner, and S. L. Sondhi, Topology and Broken Symmetry in Floquet Systems, *Annu. Rev. Condens. Matter Phys.* **11**, 345-68 (2020).

[25] M. S. Rudner and N. H. Lindner, Band structure engineering and non-equilibrium dynamics in Floquet topological insulators, *Nat. Rev. Phys.* **2**, 229 (2020).

[26] T. Kitagawa, Topological phenomena in quantum walks: elementary introduction to the physics of topological phases, *Quantum Inf Process* **11**, 1107-1148 (2012).

[27] K. Sacha and J. Zakrzewski, Time crystals: a review, *Rep. Prog. Phys.* **81**, 016401 (2018).

[28] D. V. Else, C. Monroe, C. Nayak, and N. Y. Yao, Discrete Time Crystals, *Annu. Rev. Condens. Matter Phys.* **11**, 467-99 (2020).

[29] L. Guo and P. Liang, Condensed matter physics in time crystals, *New J. Phys.* **22** 075003 (2020).

[30] V. Khemani, R. Moessner, and S. L. Sondhi, A Brief History of Time Crystals, *arXiv:1910.10745*.

[31] S. Yao, Z. Yan, and Z. Wang, Topological invariants of Floquet systems: General formulation, special properties, and Floquet topological defects, *Phys. Rev. B* **96**, 195303 (2017).

[32] R. Roy and F. Harper, Periodic table for Floquet topological insulators, *Phys. Rev. B* **96**, 155118 (2017).

[33] F. Nathan and M. S. Rudner, Topological singularities and the general classification of Floquet-Bloch systems, *New J. Phys.* **17**, 125014 (2015).

[34] R. W. Bomanara and J. Gong, Simulation of Non-Abelian Braiding in Majorana Time Crystals, *Phys. Rev. Lett.* **120**, 230405 (2018).

[35] R. W. Bomanara and J. Gong, Quantum computation via Floquet topological edge modes, *Phys. Rev. B* **98**, 165421 (2018).

[36] R. W. Bomanara and J. Gong, Measurement-only quantum computation with Floquet Majorana corner modes, *Phys. Rev. B* **101**, 085401 (2020).

[37] L. Zhou and J. Gong, Non-Hermitian Floquet topological phases with arbitrarily many real-quasienergy edge states, *Phys. Rev. B* **98**, 205417 (2018).

[38] L. Zhou and J. Pan, Non-Hermitian Floquet topological phases in the double-kicked rotor, *Phys. Rev. A* **100**, 053608 (2019).

[39] L. Zhou, Non-Hermitian Floquet topological superconductors with multiple Majorana edge modes, *Phys. Rev. B* **101**, 014306 (2020).

[40] L. Zhou, Non-Hermitian Floquet phases with even-integer topological invariants in a periodically quenched two-leg ladder, *Entropy* **22**, 746 (2020).

[41] J. Pan and L. Zhou, Non-Hermitian Floquet second order topological insulators in periodically quenched lattices, *Phys. Rev. B* **102**, 094305 (2020).

[42] W. Zhao, L. Zhou, J. Liu, P. Tong, and K. Huang, Superexponential diffusion in nonlinear non-Hermitian systems, *Phys. Rev. A* **102**, 062213 (2020).

[43] L. Zhou, Y. Gu, and J. Gong, Dual topological characterization of non-Hermitian Floquet phases, *Phys. Rev. B* **103**, L041404 (2021).

[44] L. Zhou, Dynamical characterization of non-Hermitian Floquet topological phases in one dimension, *Phys. Rev. B* **100**, 184314 (2019).

[45] M. S. Rudner and L. S. Levitov, Topological Transition in a Non-Hermitian Quantum Walk, *Phys. Rev. Lett.* **102**, 065703 (2009).

[46] L. Xiao, X. Zhan, Z. Bian, K. Wang, X. Zhang, X. Wang, J. Li, K. Mochizuki, D. Kim, N. Kawakami, W. Yi, H. Obuse, B. C. Sanders and P. Xue, Observation of topological edge states in parity-time-symmetric quantum walks, *Nat. Phys.* **13**, 1117-1123 (2017).

[47] X. Zhan, L. Xiao, Z. Bian, K. Wang, X. Qiu, B. C. Sanders, W. Yi, and P. Xue, Detecting Topological Invariants in Nonunitary Discrete-Time Quantum Walks, *Phys. Rev. Lett.* **119**, 130501 (2017).

[48] M. Li, X. Ni, M. Weiner, A. Alù, and A. B. Khanikaev, Topological phases and nonreciprocal edge states in non-Hermitian Floquet insulators, *Phys. Rev. B* **100**, 045423 (2019).

[49] V. M. Vyas and D. Roy, Topological aspects of periodically driven non-Hermitian Su-Schrieffer-Heeger model, *Phys. Rev. B* **103**, 075441 (2021).

[50] G. D. Valle and S. Longhi, Spectral and transport properties of time-periodic  $\mathcal{PT}$ -symmetric tight-binding lattices, *Phys. Rev. A* **87**, 022119 (2013).

[51] C. Yuce, PT symmetric Floquet topological phase, *Eur. Phys. J. D* **69**, 184 (2015).

[52] R. de J. León-Montiel, M. A. Quiroz-Juárez, J. L. Domínguez-Juárez, R. Quintero-Torres, J. L. Aragón, A. K. Harter, and Y. N. Joglekar, Observation of slowly decaying eigenmodes without exceptional points in Floquet dissipative synthetic circuits, *Commun. Phys.* **1**, 88 (2018).

[53] J. Li, A. K. Harter, J. Liu, L. de Melo, Y. N. Joglekar, and L. Luo, Observation of parity-time symmetry breaking transitions in a dissipative Floquet system of ultracold atoms, *Nat. Commun.* **10**, 855 (2019).

[54] B. Höckendorf, A. Alvermann, and H. Fehske, Non-Hermitian Boundary State Engineering in Anomalous Floquet Topological Insulators, *Phys. Rev. Lett.* **123**, 190403 (2019).

[55] D. Chowdhury, A. Banerjee, and A. Narayan, Light-driven Lifshitz transitions in non-Hermitian multi-Weyl semimetals, *Phys. Rev. A* **103**, L051101 (2021).

[56] P. He and Z. Huang, Floquet engineering and simulating exceptional rings with a quantum spin system, *Phys. Rev. A* **102**, 062201 (2020).

[57] E. N. Blose, Floquet topological phase in a generalized  $\mathcal{PT}$ -symmetric lattice, *Phys. Rev. B* **102**, 104303 (2020).

[58] S. Longhi, Floquet exceptional points and chirality in non-Hermitian Hamiltonians, *J. Phys. A: Math. Theor.* **50**, 505201 (2017).

[59] M. Chitsaz, H. Li, F. M. Ellis, and T. Kottos, Experimental Realization of Floquet  $\mathcal{PT}$ -Symmetric Systems, *Phys. Rev. Lett.* **119**, 093901 (2017).

[60] J. Gong and Q. Wang, Stabilizing non-Hermitian systems by periodic driving, *Phys. Rev. A* **91**, 042135 (2015).

[61] Y. Cao, Y. Li, and X. Yang, Non-Hermitian bulk-boundary correspondence in a periodically driven system, *Phys. Rev. B* **103**, 075126 (2021).

[62] H. Wu and J. An, Floquet topological phases of non-Hermitian systems, *Phys. Rev. B* **102**, 041119(R) (2020).

[63] L. Ding, K. Shi, Q. Zhang, D. Shen, X. Zhang, and W. Zhang, Experimental Determination of  $\mathcal{PT}$ -Symmetric Exceptional Points in a Single Trapped Ion, *Phys. Rev. Lett.* **126**, 083604 (2021).

[64] X. Zhang and J. Gong, Non-Hermitian Floquet topological phases: Exceptional points, coalescent edge modes, and the skin effect, *Phys. Rev. B* **101**, 045415 (2020).

[65] H. Wu, B. Wang, and J. An, Floquet second-order topological insulators in non-Hermitian systems, *Phys. Rev.*

B **103**, L041115 (2021).

[66] M. Bukov, L. D’Alessio, and A. Polkovnikov, Universal high-frequency behavior of periodically driven systems: from dynamical stabilization to Floquet engineering, *Adv. Phys.* **64**, 139 (2015).

[67] N. Goldman and J. Dalibard, Periodically Driven Quantum Systems: Effective Hamiltonians and Engineered Gauge Fields, *Phys. Rev. X* **4**, 031027 (2014).

[68] A. Eckardt and E. Anisimovas, High-frequency approximation for periodically driven quantum systems from a Floquet-space perspective, *New J. Phys.* **17** 093039 (2015).

[69] D. H. Dunlap and V. M. Kenkre, Dynamic localization of a charged particle moving under the influence of an electric field, *Phys. Rev. B* **34**, 3625 (1986).

[70] K. Drese and M. Holthaus, Ultracold atoms in modulated standing light waves, *Chem. Phys.* **217**, 201 (1997).

[71] K. W. Madison, M. C. Fischer, R. B. Diener, Qian Niu, and M. G. Raizen, Dynamical Bloch Band Suppression in an Optical Lattice, *Phys. Rev. Lett.* **81**, 5093 (1998).

[72] S. Aubry and G. André, Analyticity breaking and Anderson localization in incommensurate lattices, *Ann. Israel Phys. Soc.* **3**, 133 (1980).

[73] P. G. Harper, Single band motion of conduction electrons in a uniform magnetic field, *Proc. Phys. Soc. London A* **68**, 874 (1955).

[74] J. B. Sokoloff, Unusual band structure, wave function and electrical conductance in crystals with incommensurate periodic potentials, *Phys. Rep.* **126**, 189 (1985).

[75] T. Liu, H. Guo, Y. Pu, and S. Longhi, Generalized Aubry-André self-duality and mobility edges in non-Hermitian quasiperiodic lattices, *Phys. Rev. B* **102**, 024205 (2020).

[76] S. Longhi, Topological Phase Transition in non-Hermitian Quasicrystals, *Phys. Rev. Lett.* **122**, 237601 (2019).

[77] S. Longhi, Metal-insulator phase transition in a non-Hermitian Aubry-André-Harper model, *Phys. Rev. B* **100**, 125157 (2019).

[78] S. Longhi, Phase transitions in a non-Hermitian Aubry-André-Harper model, *Phys. Rev. B* **103**, 054203 (2021).

[79] H. Jiang, L. Lang, C. Yang, S. Zhu, and S. Chen, Interplay of non-Hermitian skin effects and Anderson localization in nonreciprocal quasiperiodic lattices, *Phys. Rev. B* **100**, 054301 (2019).

[80] Y. Liu, X.-P. Jiang, J. Cao, and S. Chen, Non-Hermitian mobility edges in one-dimensional quasicrystals with parity-time symmetry, *Phys. Rev. B* **101**, 174205 (2020).

[81] Y. Liu, Y. Wang, Z. Zheng, and S. Chen, Exact non-Hermitian mobility edges in one-dimensional quasicrystal lattice with exponentially decaying hopping and its dual lattice, *Phys. Rev. B* **103**, 134208 (2021).

[82] Y. Liu, Y. Wang, X. Liu, Q. Zhou, and S. Chen, Exact mobility edges, PT-symmetry breaking, and skin effect in one-dimensional non-Hermitian quasicrystals, *Phys. Rev. B* **103**, 014203 (2021).

[83] Z. Xu and S. Chen, Dynamical evolution in a one-dimensional incommensurate lattice with PT symmetry, *Phys. Rev. A* **103**, 043325 (2021).

[84] Q. Zeng, S. Chen, and R. Lü, Anderson localization in the non-Hermitian Aubry-André-Harper model with physical gain and loss, *Phys. Rev. A* **95**, 062118 (2017).

[85] X. Cai, Boundary-dependent self-dualities, winding numbers, and asymmetrical localization in non-Hermitian aperiodic one-dimensional models, *Phys. Rev. B* **103**, 014201 (2021).

[86] A. Jazaeri and I. I. Satija, Localization transition in incommensurate non-Hermitian systems, *Phys. Rev. E* **63**, 036222 (2001).

[87] Q. Zeng, Y. Yang, and R. Lü, Topological phases in one-dimensional nonreciprocal superlattices, *Phys. Rev. B* **101**, 125418 (2020).

[88] Q. Zeng, Y. Yang, and Y. Xu, Topological phases in non-Hermitian Aubry-André-Harper models, *Phys. Rev. B* **101**, 020201(R) (2020).

[89] L. Tang, G. Zhang, L. Zhang, and D. Zhang, Localization and topological transitions in non-Hermitian quasiperiodic lattices, *Phys. Rev. A* **103**, 033325 (2021).

[90] T. Liu, S. Cheng, H. Guo, and X. Gao, Fate of Majorana zero modes, exact location of critical states, and unconventional real-complex transition in non-Hermitian quasiperiodic lattices, *Phys. Rev. B* **103**, 104203 (2021).

[91] L. Zhai, G. Huang, and S. Yin, Cascade of the delocalization transition in a non-Hermitian interpolating Aubry-André-Fibonacci chain, arXiv:2104.06035.

[92] Q. Zeng and Y. Xu, Winding numbers and generalized mobility edges in non-Hermitian systems, *Phys. Rev. Res.* **2**, 033052 (2020).

[93] X. Xia, K. Huang, S. Wang, and X. Li, A new class of exact mobility edges in non-Hermitian quasiperiodic models, arXiv:2105.12640.

[94] In preparation.